Mudrock fractures characterization from well logs. AVO and AVAz analysis of the Quintuco-Vaca Muerta system and the Vaca Muerta-Tordillo system in the oil maturity window.

Ariel Sánchez Camus[*]   Patricia M. Gauzellino[†]   Ricardo Ramos[‡]

Juan E. Santos[§]

November, 2018

Abstract

The present technologies for the acquisition and processing of seismic data such as cross-dipole sonic profiles, VSPs walkaround and walkaway, or seismic multicomponent (3C) allow to measure wave propagation in different directions. This way, by making an analysis of velocity, attenuation, AVO or AVAz, a mechanical characterization of the medium anisotropy is obtained. The following work presents an analysis of wave propagation in Vaca Muerta. The different seismic behaviours, depending on the elastic symmetry and the reflection coefficient of the systems (Quintuco-Vaca Muerta and Vaca Muerta-Tordillo), are studied. Following this objective, a new tool based on the Finite Element Method (FEM) was developed, which allows the simulation of a full wave propagation (wave conversion modes). This simulation process generates synthetic seismograms, which are sensitive to the medium anisotropy. It also allows to build velocity models with higher accuracy for the calibration of several kinds of the acquisitions mentioned above. For instance, the prediction of location and focal mechanisms of the micro seismic source can be established by comparing synthetic seismogram (full wave inversion) with the seismogram recorded in field.

Keywords: fractures, well logs, mudrock, anisotropy, AVO, AVAz, Vaca Muerta

[*]Tections, Calle 31 No 1905, La Plata (1900), Argentina, Departamento de Geofísica Aplicada, Facultad de Ciencias Astronómicas y Geofísicas, Universidad Nacional de La Plata, Paseo del Bosque s/n, La Plata (1900), Argentina.
E-mail address: acamus@tections.com, acamus@fcaglp.unlp.edu.ar

[†]Departamento de Geofísica Aplicada, Facultad de Ciencias Astronómicas y Geofísicas, Universidad Nacional de La Plata, Paseo del Bosque s/n, La Plata (1900), Argentina.
E-mail address: gauze@fcaglp.unlp.edu.ar

[‡]Tections, Calle 31 No 1905, La Plata (1900), Argentina, ,Facultad de Ingeniería, Universidad Nacional de La Plata,Calle 1 y 47, La Plata (1900), Argentina.
E-mail address: rramos@tections.com

[§]Instituto del Gas y del Petróleo, Facultad de Ingeniería, Universidad de Buenos Aires, Buenos Aires, Argentina, Department of Mathematics, Purdue University, W. Lafayette, IN 47907-2067, USA.
E-mail address: santos@math.purdue.edu

1 Introduction

Velocity inversion and amplitude inversion are techniques widely used in the Oil and Gas industry. Velocity inversion generates a velocity-depth earth model, which is common practice in the sequence of processing and interpretation of seismic data (e.g, migration, stacking, seismic-to-well tie). On the other hand, amplitude inversion uses the arrival time and the amplitude of the reflected seismic waves to solve the relative impedances among seismic reflectors. In formations with a high anisotropy degree, such as mudrocks or conventional fractured reservoirs, these attributes vary considerably between interfaces. Therefore, in order to have an accurate interpretation of the seismic inversion, the anisotropy of the formations should not be ignored. The following work presents a modeling tool based on a finite element numerical method ([11], [12], [30], [31]). The simulation of full wave propagation (including conversion modes) allows to generate synthetic seismograms for media with different types of anisotropy. Taking into account these concepts, an analysis of full wave propagation on the systems Quintuco-Vaca Muerta and Vaca Muerta-Tordillo is presented and comparisons among seismic responses for isotropic and anisotropic models are made.

2 Elastic parameters estimation

In order to characterize the full elastic tensor of the formations, three complete sets of acoustic logging measurements were used, together with petrophysical logs, geological maps, seismic cubes and microseismic data ([37],[24],[48]). The equivalent VTI medium for each formation is represented by the stiffnesses calculated from Backus averaging as shown in Appendix A, and B. The compliances and the resulting stiffness matrix, when assuming two sets of orthogonal fractures embedded in the VTI background, are obtained using the model proposed by Carcione et al. ([5]). The stiffness matrix can also be obtained from other types of seismic acquisitions. For instance, Curcio et al. ([9]) and Curia et al. ([10]) obtain these parameters from VSPs walkaround and VSPs walkaway acquisitions.

3 Mudrock fracture characterization

The low energy conditions of the depositional environment of organic-rich mudrocks favors a parallel-bedded accommodation of the clay platelets and the organic matter (OM). These distributions of clay minerals, silt and OM, in addition to the presence of thin veins of fibrous calcite parallel to bedding (Beef fractures), result in an elastic symmetry that can be approximated by a vertical transversely isotropic (VTI) medium, which is characterized by its density and five independent constants. In this elastic symmetry, the rotational axis is perpendicular to the earth surface, which implies that the material properties are directionally invariant in the horizontal plane ([43], [25], [45], [46], [40], [7], [33], [38], [41]). The stiffness matrix for a VTI symmetry is:

$$\mathbf{C} = \begin{pmatrix} c_{11} & c_{12} & c_{13} & 0 & 0 & 0 \\ c_{12} & c_{11} & c_{13} & 0 & 0 & 0 \\ c_{13} & c_{13} & c_{33} & 0 & 0 & 0 \\ 0 & 0 & 0 & c_{55} & 0 & 0 \\ 0 & 0 & 0 & 0 & c_{55} & 0 \\ 0 & 0 & 0 & 0 & 0 & c_{66} \end{pmatrix}$$

where,

$$c_{12} = c_{11} - 2c_{66}.$$

The anisotropy and the compliance of the mudrocks is enhanced if a dense set of fluid filled-fractures is present ([13],[14],[6],[33], [36],[42]). The contrast between the soft material infill and the background stiffness results in an orthorhombic or monoclinic elastic symmetry.

In order to obtain the compliance matrix $\mathbf{Z}$ and the resulting fractured mudrock matrix $\mathbf{P}$, the model proposed by Carcione et al.([5]) is used and the conversion factor Λ is introduced. The proposed methodology can be applied to get the compliance of a fracture set that has a dominant direction over the rest (single fracture set), or two dominant perpendicular directions (two fractures sets). See Figure 1. The resulting medium consists of sets of vertical fractures embedded in a VTI background medium to form a long-wavelength equivalent orthorrombic medium. Long-wavelength equivalent means that the dominant wavelength of the signal is much longer than the fracture spacing ([34]). The computation of the compliance matrix can be derived by carrying out the matrix multiplication given by Nichols et al. ([21]) or directly using 4th-rank tensor notation. Carcione et al. ([5]) have introduced $Z_N = Z_1/L$, $Z_H = Z_2/L$, and $Z_V = Z_3/L$, where Z_1 is the normal compliance, Z_2 is the horizontal tangential compliance, Z_3 is the vertical tangential compliance, and L is the average fracture spacing.
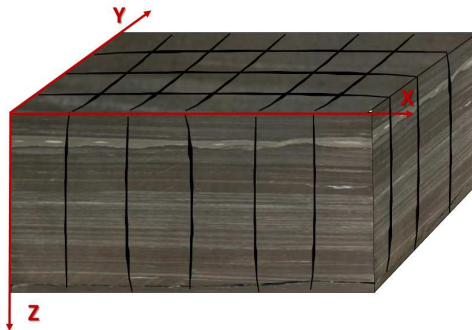

Figure 1: Fractured Mudrock.

An orthorhombic medium described in its natural reference system (NRS) has three planes of symmetry. Therefore, in order to decribe the fractured mudrock in its NRS, one set strike is along the y-direction and the other is along the x-direction (Figure 1). The fracture stiffness matrixes are given by

$$\mathbf{S_f}^{(1)} = \begin{pmatrix} Z_N^{(1)} & 0 & 0 & 0 & 0 & 0 \\ 0 & 0 & 0 & 0 & 0 & 0 \\ 0 & 0 & 0 & 0 & 0 & 0 \\ 0 & 0 & 0 & 0 & 0 & 0 \\ 0 & 0 & 0 & 0 & Z_V^{(1)} & 0 \\ 0 & 0 & 0 & 0 & 0 & Z_H^{(1)} \end{pmatrix}$$

for the set parallel to the y-axes and

$$\mathbf{S_f}^{(2)} = \begin{pmatrix} 0 & 0 & 0 & 0 & 0 & 0 \\ 0 & Z_N^{(2)} & 0 & 0 & 0 & 0 \\ 0 & 0 & 0 & 0 & 0 & 0 \\ 0 & 0 & 0 & Z_V^{(2)} & 0 & 0 \\ 0 & 0 & 0 & 0 & 0 & 0 \\ 0 & 0 & 0 & 0 & 0 & Z_H^{(2)} \end{pmatrix}$$

for the set parallel to the x-axes.

From now on, the VTI elastic parameters are referred to as c_{ij} and the orthorhombic elastic parameters as p_{ij}.

In the (three) symmetry planes of an orthorhombic medium, there is a pure shear wave and two coupled waves ([6]). The fast pure shear wave velocity and the slow pure shear wave velocity are along the principal axes on the (x, y)-plane. Therefore, the p_{44} and the p_{55} coefficients can be obtained from the sonic cross-dipole tool.

Combining the acoustic logging measurements the c_{66}, c_{55} and the c_{33} for the unfractured mudrock, and the p_{66}, p_{44}, p_{55}, and the p_{33} for the fractured mudrock are obtained. See Figure 2.
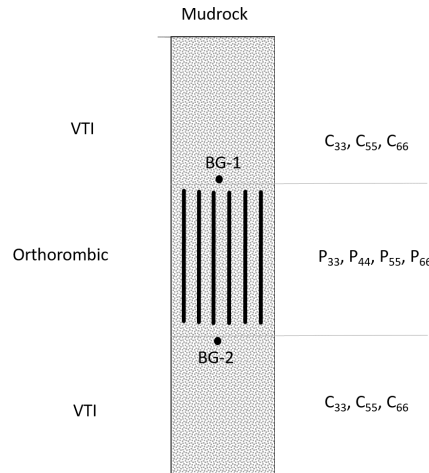

Figure 2: Borehole-Mudrock Intervals.

In order to compute the fractures compliances, a representative VTI background of the fractured zone must be chosen. The preliminary intervals to calculate the VTI background

should be picked above (BG-1) and below (BG-2) the fractured zone. Then, the equivalent VTI background is computed using Backus average between these intervals ([4],[7]). Note that the presence of a more compliant material reduces the elastic coefficients; hence, the c_{ij} must be greater than the p_{ij}. Once the VTI background is obtained, the compliances $Z_V^{(1)}$, $Z_V^{(2)}$ and $Z_H^{(1)}+Z_H^{(2)}$ are calculated from p_{44}, p_{55}, p_{66}, c_{55}, and c_{66} coefficients using the Carcione et al.([5]) model,

$$Z_V^{(1)} = \frac{1}{p_{55}} - \frac{1}{c_{55}}, Z_V^{(2)} = \frac{1}{p_{44}} - \frac{1}{c_{55}}, Z_H^{(1)} + Z_H^{(2)} = \frac{1}{p_{66}} - \frac{1}{c_{66}}.$$

To obtain the $Z_N^{(1)}$ and the $Z_N^{(2)}$ compliances from p_{33} and the VTI background, the underdetermined equation (3.1) must be solved. In order to solve this equation the conversion factor Λ is introduced.

$$Z_N^{(1)} + Z_N^{(2)} = \frac{c_{33} - p_{33} + Z_N^{(1)} Z_N^{(2)} [(c_{33} - p_{33})(c_{11}^2 - c_{12}^2) - 2c_{13}^2(c_{11} - c_{12})]}{p_{33}c_{11} - c_{11}c_{33} + c_{13}^2}. \tag{3.1}$$

Since the only two independent estimations of the compliances come from the pure shear wave, the factor Λ measures the difference between $Z_V^{(1)}$ and $Z_V^{(2)}$ and expresses one as a linear combination of the other. Supposing that $Z_V^{(i)}$ is greater than $Z_V^{(j)}$, then the conversion factor Λ is:

$$\Lambda = 1 - \left(\frac{Z_V^{(i)} - Z_V^{(j)}}{Z_V^{(i)}} \right),$$

hence,

$$Z_V^{(j)} = \Lambda Z_V^{(i)}.$$

Assuming that Λ is the same for the rest of the compliances, $Z_N^{(1)}$ and $Z_N^{(2)}$ can be obtained. When applying the conversion factor, the equation (3.1) is reduced to a quadratic equation (3.2). Taking the positive solution as valid, both normal compliances are obtained.

$$a(Z_N^{(i)})^2 + bZ_N^{(i)} + c = 0, \tag{3.2}$$

where

$$a = \Lambda[2c_{13}^2(c_{11} - c_{12}) - c_{33}(c_{11}^2 - c_{12}^2)],$$

$$b = (1 + \Lambda)(p_{33}c_{11} - c_{11}c_{33} + c_{13}^2),$$

$$c = p_{33} - c_{33},$$

then,

$$Z_N^{(j)} = \Lambda Z_N^{(i)}.$$

The horizontal tangential compliances are computed using factor Λ as well,

$$Z_H^{(i)} = \frac{c_{66} + p_{66}}{c_{66}p_{66}(1 + \Lambda)},$$

hence,

$$Z_H^{(j)} = \Lambda Z_H^{(i)}.$$

Once both sets of fractures compliances are obtained, the remaining p_{ij} are calculated to complete the orthorhombic matrix.

$$p_{11} = \frac{c_{11} + Z_N^{(2)}(c_{11}^2 - c_{12}^2)}{1 + Z_N^{(1)} Z_N^{(2)}(c_{11}^2 - c_{12}^2) + c_{11}(Z_N^{(1)} + Z_N^{(2)})},$$

$$p_{12} = \frac{c_{12}}{1 + Z_N^{(1)} Z_N^{(2)}(c_{11}^2 - c_{12}^2) + c_{11}(Z_N^{(1)} + Z_N^{(2)})},$$

$$p_{13} = \frac{c_{13}[1 + Z_N^{(2)}(c_{11} - c_{12})]}{1 + Z_N^{(1)} Z_N^{(2)}(c_{11}^2 - c_{12}^2) + c_{11}(Z_N^{(1)} + Z_N^{(2)})},$$

$$p_{22} = \frac{c_{11} + Z_N^{(1)}(c_{11}^2 - c_{12}^2)}{1 + Z_N^{(1)} Z_N^{(2)}(c_{11}^2 - c_{12}^2) + c_{11}(Z_N^{(1)} + Z_N^{(2)})},$$

$$p_{23} = \frac{c_{13}[1 + Z_N^{(1)}(c_{11} - c_{12})]}{1 + Z_N^{(1)} Z_N^{(2)}(c_{11}^2 - c_{12}^2) + c_{11}(Z_N^{(1)} + Z_N^{(2)})}.$$

If the compliances parameters were calculated correctly, the values p_{33}, p_{44}, p_{55}, and p_{66} measured by the sonic logs should be equal to:

$$p_{33} = \frac{c_{33} + (Z_N^{(1)} + Z_N^{(2)})(c_{11}c_{33} - c_{13}^2) + Z_N^{(1)} Z_N^{(2)}(c_{11} - c_{12})[c_{33}(c_{11} + c_{12}) - 2c_{13}^2]}{1 + Z_N^{(1)} Z_N^{(2)}(c_{11}^2 - c_{12}^2) + c_{11}(Z_N^{(1)} + Z_N^{(2)})},$$

$$p_{44} = \frac{c_{55}}{1 + c_{55}Z_V^{(2)}},$$

$$p_{55} = \frac{c_{55}}{1 + c_{55}Z_V^{(1)}},$$

$$p_{66} = \frac{c_{66}}{1 + c_{66}(Z_H^{(1)} + Z_H^{(2)})}.$$

Then, the orthorhombic equivalent medium for the fractured mudrock is:

$$\mathbf{P} = \begin{pmatrix} p_{11} & p_{12} & p_{13} & 0 & 0 & 0 \\ p_{12} & p_{22} & p_{23} & 0 & 0 & 0 \\ p_{13} & p_{23} & p_{33} & 0 & 0 & 0 \\ 0 & 0 & 0 & p_{44} & 0 & 0 \\ 0 & 0 & 0 & 0 & p_{55} & 0 \\ 0 & 0 & 0 & 0 & 0 & p_{66} \end{pmatrix}.$$

4 Seismic and Geological Characteristics of the Study Area

The study area is in the Loma Jarillosa Este (LJE) block, which is located in the Vaca Muerta (VM) oil/wet-gas generation window. See Figure 3.
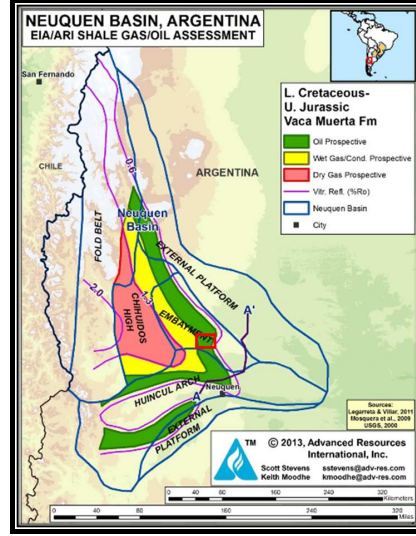

Figure 3: The study area is marked by a red rectangle-ARI map 2013.

In this region VM formation has an average thickness of 100 meters and its base is located between 2500 m and 3000 m deep. The mineralogical composition is comprised mainly of calcite, quartz, feldspar, and several clay minerals, with the majority of the clay being illite, mica and the mixed illite/smectite phase. The upper and middle VM sections were classified as argillaceous marlstones and the lower VM section as a siliceous marlstone. The TOC content ranges between 3% to 12% and the kerogen is primarily type II ($0.6\% < R_o < 1.23\%$). The average porosity is 7% and the permeability ranges from 61 nD to 218 nD. The overlying Quintuco formation (shallow marine facies) is mainly a limestone reservoir with some dolomite and anhydrite, while the underlying Tordillo formation is a clastic reservoir deposited through eolian and lacustrine mechanisms ([16]).

In the Table 1, v_{p0}, v_{s0}, v_{p90} and v_{s90} are the velocities along the vertical and the horizontal axes; ρ is the rock density; K is the kerogen content; ε, γ, and δ are the Thomsen's parameters; A_p and A_s are the P-wave anisotropy and the S-wave anisotropy; Y_i, and ν_i are the Young's modulus and the Poisson's ratios (i=1,2,3). The kerogen volume fraction was calculated with the relationship obtained by Vernick and Milovac ([47]) from the mass-balance equation.

	$QUINTUCO$	UVM	LVM	$TORDILLO$
v_{p0} (m/s)	4425.92	3671.13	3271.71	4591.99
v_{p90} (m/s)	5447.19	4497.33	4104.17	4620.59
v_{s0} (m/s)	2554.32	2136.46	1921.18	2606.25
v_{s90} (m/s)	2842.48	2357.78	2210.71	2631.41
ρ (kg/m^3)	2663	2590	2495	2608
K (vol/vol)	-	5 %	15 %	-
ε	0.26	0.25	0.29	$6.25\text{x}10^{-3}$
γ	0.12	0.11	0.16	$9.7\text{x}10^{-3}$
δ	0.25	0.25	0.25	$-2.85\text{x}10^{-8}$
A_p $(\%)$	18.74	18.4	20.28	0.619
A_s $(\%)$	10.13	9.4	13.09	0.95
Y_1 (Gpa)	45.81	31.15	23.84	44.59
Y_2 (Gpa)	47.82	32.38	25.28	44.77
Y_3 (Gpa)	43.44	29.52	22.77	44.64
ν_1	0.318	0.317	0.294	0.258
ν_2	0.376	0.369	0.372	0.263
ν_3	0.25	0.248	0.236	0.259

Table 1: Dynamic elastic parameters under reservoir conditions.

The non-organic Quintuco mudrock presents moderate to strong anisotropy (VTI), while the Tordillo sandstone is isotropic. As can be seen in Table 1, VM formation is a low velocity zone of moderate to strong anisotropy (VTI) between these formations. The velocity reversal from top to base takes places because in the hydrocarbon generation window organic-rich mudrocks are overpressured. Hydrocarbon generation processes cause bedding-parallel microcracks, develop organopores and transfer load to the rock squeleton ([44], [20], [46], [1]). As the pore space volume increases, the wave velocities decrease and the degree of anisotropy increases ([7], [23], [50], [2]).

5 Full Wave Propagation: Fractured Middle Vaca Muerta.

In this section, a full wave propagation of a fractured calcareous VM is presented. The interval selected for the simulation is an oil-brine saturated corridor. The fracture geometry in this zone is dominated by two perpendicular sets. In order to describe the fractured mudrock in its NRS, one fracture strike is considered along the y-direction and the other strike along the x-direction. Both directions are related to the minimum and maximum horizontal stress and the weakness planes directions (related to the zone normal faulting). These orientations have been estimated from borehole breakouts, drilling-induced fractures, and the World Stress Map database ([15]).

The fractured VM corridor is characterized by ρ=2567 Kg/m^3 and the following orthorhombic stiffness matrix (Gpa):

$$\mathbf{P} = \begin{pmatrix} 35.770 & 13.540 & 13.222 & 0 & 0 & 0 \\ 13.540 & 39.833 & 14.31 & 0 & 0 & 0 \\ 13.222 & 14.31 & 37.064 & 0 & 0 & 0 \\ 0 & 0 & 0 & 13.323 & 0 & 0 \\ 0 & 0 & 0 & 0 & 13.014 & 0 \\ 0 & 0 & 0 & 0 & 0 & 12.353 \end{pmatrix}.$$

Figure 4 shows a 3D wave propagation caused by the vertical perturbation of a 25 hz Ricker wavelet. As expected, different wave-fronts propagate for each symmetry plane.
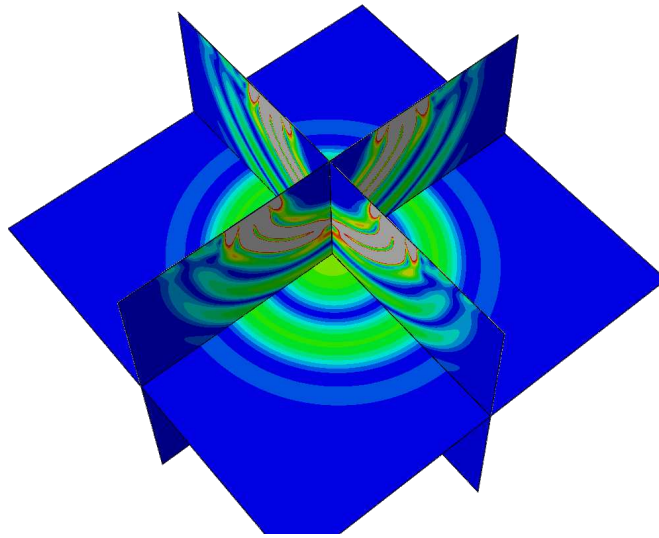

Figure 4: Velocity magnitud in the symmetry planes.

As can be seen in the Table 2, the open fracture set along the y-axis is denser than the set along the x-axis. The x-direction is along the fault-related weakness planes and the current minimum horizontal stress. These results are in agreement with the microseismic events occurrence and the production logs.

Table 2 shows the velocities along the principal axes for each symmetry plane.

Plane	(x,y)	(x,z)	(y,z)
$v_{qP(0°)}$	3939.229 m/s	3799.860 m/s	3799.860 m/s
$v_{qP(90°)}$	3732.919 m/s	3732.919 m/s	3939.229 m/s
$v_{qS(0°)}$	2193.712 m/s	2251.591 m/s	2278.182 m/s
$v_{qS(90°)}$	2193.712 m/s	2251.591 m/s	2278.182 m/s
$v_{S(0°)}$	2278.182 m/s	2278.182 m/s	2193.712 m/s
$v_{S(90°)}$	2251.591 m/s	2193.712 m/s	2251.591 m/s

Table 2: VM Orthorhombic Velocities in the symmetry planes.

Figure 5 shows the qP-wave velocity variation as a function of the phase angle and the

azimuth angle. The 0° azimuth is along the y-axis direction and the 90° azimuth is along the x-axis direction.
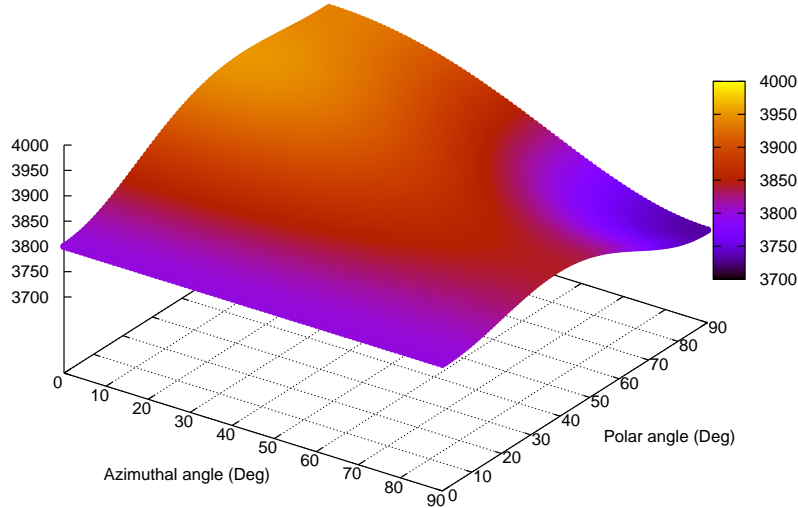

Figure 5: Surface plot of qP-wave velocity as a function the incidence angle and the azimuthal angle.

The validation of the computational code is shown in Appendix C.

6   AVO and AVAz analysis.

The convolutional model of the seismic trace is the basic model which is based on many seismic inversion methods. It states that the seismic trace is the convolution of the wavelet with the earth's reflectivity series, with the addition of a noise component ([29]). The inversion can be performed before stacking or after stacking. Stacking produces a single trace with a signal amplitude equal to the average of the signal in the stacked traces. If the medium velocity and the offset amplitude variation change gradually, these assumptions are valid, and inversion may be performed on the poststack data. Otherwise, these assumptions do not hold, and inversion is applied to prestack data (AVO or AVAz analysis). Several approximations have been made to determine the reflection coefficients as a function of a certain range of incidence angles. These linearized approximations of the P-wave reflection coefficient, as well as the Zoeppritz equations ([51]), assume that the rocks are an isotropic medium. Rüger ([28]) stated that any changes in anisotropy have a strong influence on the reflection coefficients. The purpose of the following analysis is to determine the difference (if there is one at all) between the isotropic and the anisotropic model using the Rüger approximation.

6.1 P-wave reflection coefficient of the Quintuco-VM system.

Figure 6 shows the AVO variation for the Quintuco-VTI/VM-VTI configuration, and its equivalent isotropic configuration (Quintuco-ISO/VM -ISO). This graphic illustrates the difference between the anisotropic model and the isotropic model.
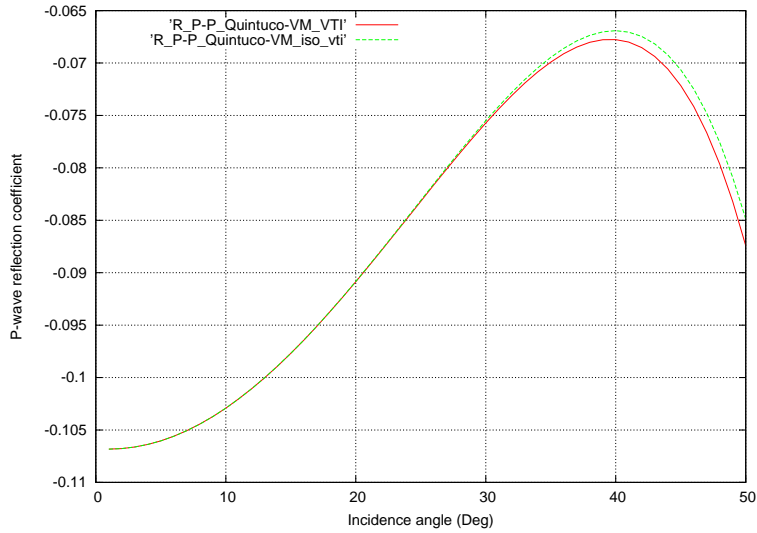

Figure 6: VTI vs Isotropic AVO model.

Figure 7 shows the AVAz variation for the Quintuco-Orthorhombic/VM-Orthorhombic system, and their equivalent isotropic configurations. In this case, the set along the x-axis (90° azimuth) is denser than the set along the y-axis (0° azimuth).
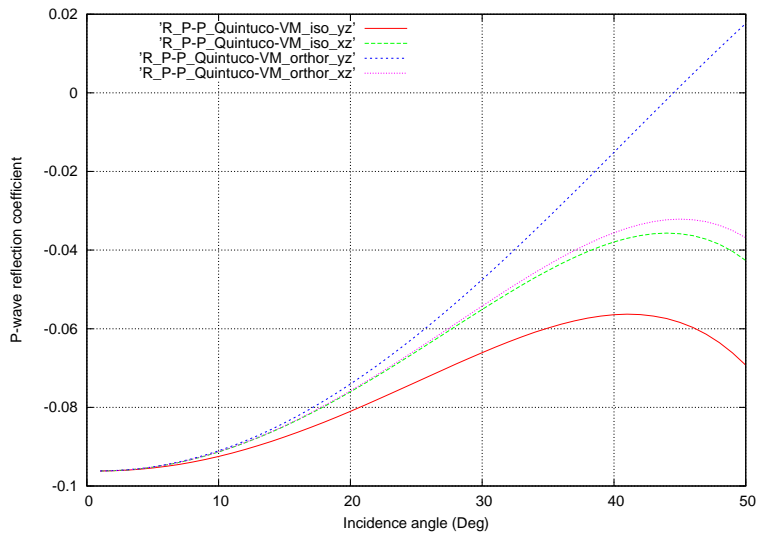
Figure 7: Orthorhombic vs Isotropic AVO models.

Figure 8 shows the P-wave reflection coefficient as a function of the incidence angle and the azimuthal angle.
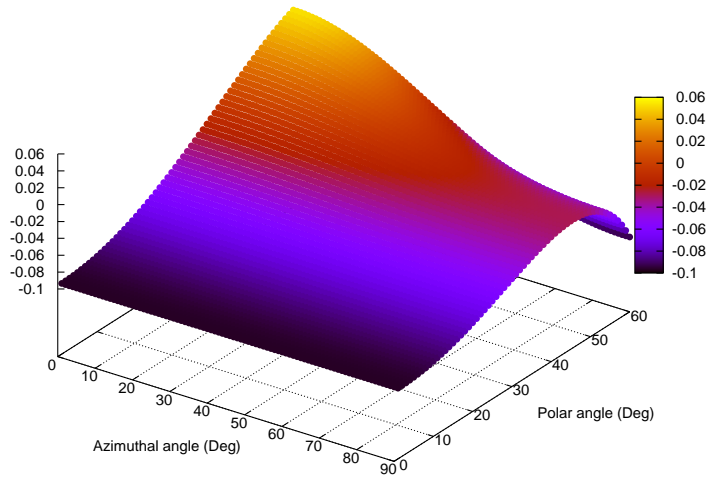

Figure 8: Surface plot of the Rpp coefficient for Quintuco-Orthorhombic/VM-Orthorhombic configuration.

6.2   P-wave reflection coefficient of the VM-Tordillo system.

Figure 9 illustrates the AVO variation for the VM-VTI/Tordillo-VTI configuration, and its equivalent isotropic configuration.
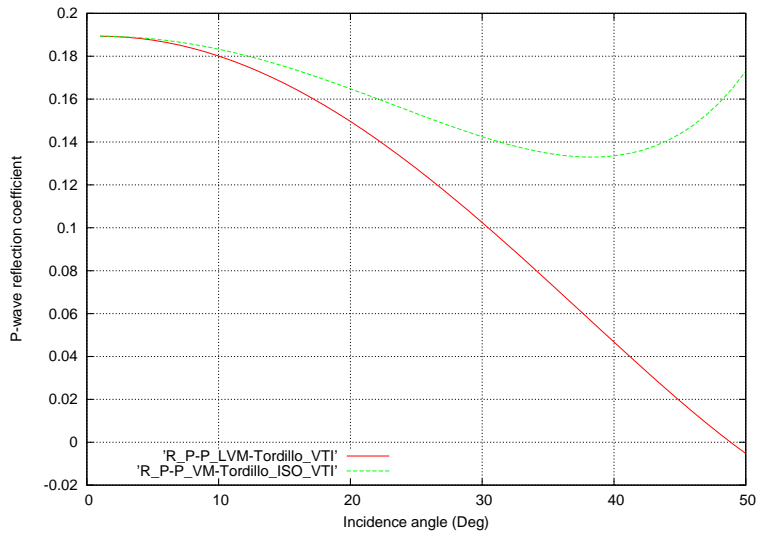

Figure 9: VTI vs Isotropic AVO model.

Figure 10 shows the AVAz variation for the VM-Orthorhombic/Tordillo-Orthorhombic system, and their isotropic equivalent configurations. The set along the x-axis (90° azimuth) is denser than the set along the y-axis (0° azimuth).
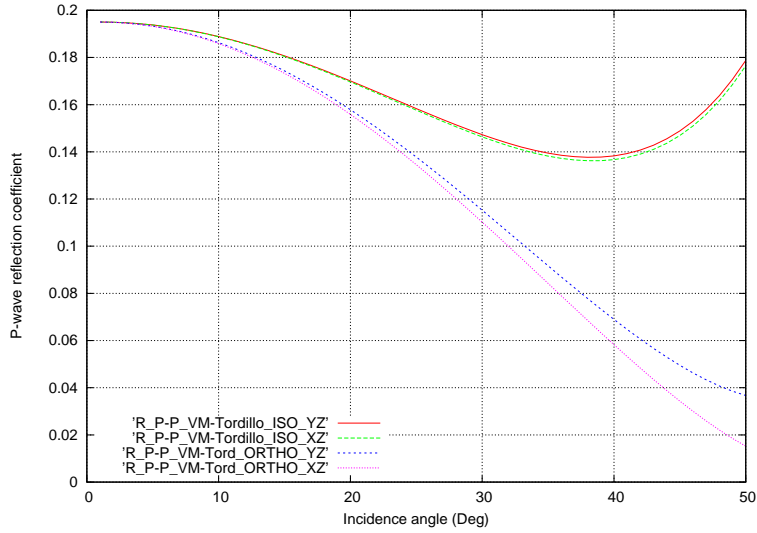

Figure 10: Orthorhombic vs Isotropic AVO models.

Figure 11 shows the P-wave reflection coefficient as a function of the incidence angle and the azimuthal angle.
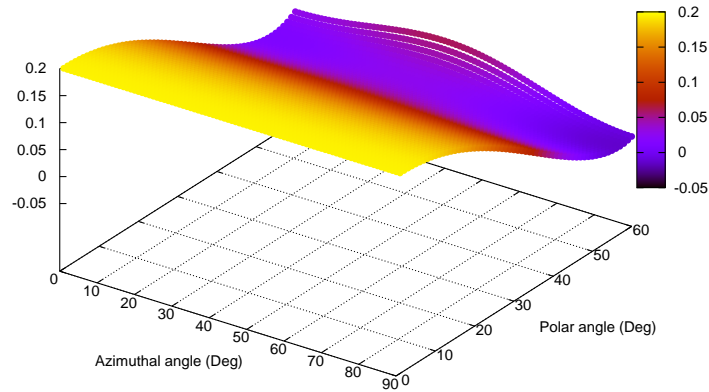

Figure 11: Surface plot of the Rpp coefficient for VM-Orthorhombic/Tordillo-Orthorhombic configuration.

7 Conclusions.

The velocities models along with the AVO, and the AVAz models performed for this study, have shown that ignoring the anisotropy in the Quintuco-Vaca Muerta, and the Vaca Muerta-Tordillo systems can lead to significant mistakes in the interpretation of the seismic data, and the geomechanical parameters estimation. Therefore, when developing complex reservoirs, an anisotropy model is needed in order to minimize errors. The simulation, and the characterization processes generate synthetic seismograms, which are sensitive to the medium anisotropy. This allows to build models with higher accuracy for the calibration of several kinds of seismic acquisitions.

8 Appendix A: Full transversely isotropic elastic tensor.

In order to determine a full transversely isotropic (TI) elastic tensor from acoustic logging measurements in the field, a cross-dipole, a dipole or a monopole sonic tool are required ([37], [24], [48]). See Figure 12 modified from Sinha et al. ([37]).
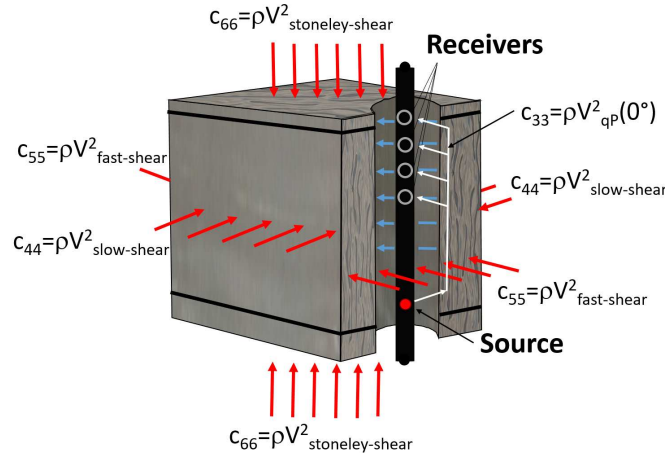

Figure 12: Vertical well-Acoustic Logging Measurements.

The two vertical shear moduli c_{44} and c_{55} in an anisotropic formation with a vertical z-axis are obtained from crossed-dipole sonic data, whereas the horizontal shear modulus c_{66} is estimated from borehole Stoneley data (only in vertical wells).

From the slowness curves and the bulk density ρ, four of the five elastic stiffness coefficients necessary to define a TI medium are calculated. Note that for a VTI medium ($c_{44}=c_{55}$) there is no S-wave split on the horizontal plane (isotropic plane).

$$c_{33} = \rho V_{qP}^2(0°),$$
$$c_{44} = \rho V_{slow-shear}^2,$$
$$c_{55} = \rho V_{fast-shear}^2,$$
$$c_{66} = \rho V_{stoneley-shear}^2.$$

The elastic constants c_{13} and c_{12} can be determined from the ANNIE method or the MANNIE method. The ANNIE method assumes that the Thomsen' parameter δ is equal to zero ([35],[32]). Then,

$$c_{13} = c_{33} - 2c_{44},$$
$$c_{12} = c_{13}.$$

The MANNIE method uses core measurements to determine a relationship between these parameters. In this method, cores taken parallel to, perpendicular to, and at 45° from the bedding direction are used to obtain the coefficients ζ and ξ ([49]).Then,

$$c_{13} = \zeta c_{33} - 2c_{44},$$
$$c_{12} = \xi c_{13}.$$

In order to obtain the coefficient c_{11}, an equation of symmetry is used ([6]).

$$c_{11} = c_{12} + 2c_{66}.$$

9   Appendix B: Backus averaging.

The five stiffnesses c_{ij} for a VTI equivalent medium are calculated by applying Backus average,

$$\bar{c}_{33} = \langle c_{33}^{-1} \rangle^{-1},$$
$$\bar{c}_{55} = \langle c_{55}^{-1} \rangle^{-1},$$
$$\bar{c}_{13} = \langle c_{33}^{-1} \rangle^{-1} \langle c_{33}^{-1} c_{13} \rangle,$$
$$\bar{c}_{11} = \langle c_{11} - c_{13}^2 c_{33}^{-1} \rangle + \langle c_{33}^{-1} \rangle^{-1} \langle c_{33}^{-1} c_{13} \rangle^2,$$
$$\bar{c}_{66} = \langle c_{66} \rangle,$$
$$\bar{\rho} = \langle \rho \rangle.$$

where the c_{ij} stifnesses correspond to the single layers, and $\langle . \rangle$ indicates the thickness weighted average.

At low frequencies, Backus's theory is valid when the dominant wavelength of the signal is much larger than the thickness of the layers composing the medium. An acceptable guideline is that the wavelength must be larger than eight times the layer thickness ([6]). Lindsay and Koughnet ([18]) implemented Backus average sequentially and at small depth increments for upscaling well logs to seismic wavelengths. The size of the upscaling window is found by estimating the temporal wavelet length from the seismic bandwidth and the average velocity. This technique upscales log measurements to seismic wavelengths preserving gradational interfaces and rock properties without introducing artificial blocks (blocked velocity model). However, the effect of partial saturation on velocity depends on the frequency range ([3],[7]). At low frequencies, the fluid has enough time to achieve pressure equilibration (relaxed regime), whereas at high frequencies the fluid can not relax. This state of unrelaxation induces a stiffening of the pore material; hence, the velocities obtained might be overstimated.

10 Appendix C: Propagation Wave Simulation.

The full wave propagation simulation code solves the movement equation (10.3) by applying the Finite Element Method (FEM) in the explicit domain,

$$\rho(\mathbf{x})\frac{\partial^2 u_i}{\partial t^2} - \frac{\partial}{\partial x_j}\left(c_{ijkl}\frac{\partial u_l}{\partial x_k}\right) = f(\mathbf{x}, t) \quad (i, j, k, l = 1, 2, 3) , \qquad (10.3)$$

where c_{ijkl} is the stiffness matrix, u_i indicates the displacement components, $\rho(\mathbf{x})$ the density, and $f(\mathbf{x}, t)$ is the external source. The code was validated by comparing it to the 3D analytical solution published by Carcione 2015 ([6]), and by reproducing the Li model ([17]), the Ostrander model ([22]), and the Schoenberg and Helbig ([36]) model ([30], [31]), see Figure 13.
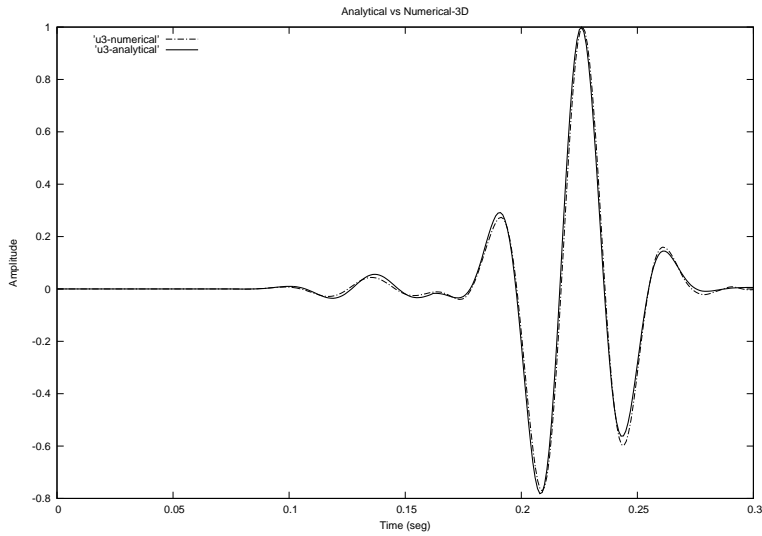
Figure 13: u_z numerical vs u_z analitical solution.

11   Acknowledgments.

References

[1] Al Duhailan M.A, Sonnenberg S.A., Meckel L.D, 2013 *Insights on Hydrocarbon-Generation Microfracturing in Organic-Rich Shales.* SPE 168667 / URTeC 1515553.

[2] Allan A.M., Vanorio T., Dahl J.P, 2014 *Pyrolysis-induced P-wave velocity anisotropy in organic-rich shales.* Geophysics, 79, no. 2 ; P. D41D53, doi:10.1190/GEO2013-0254.1.

[3] Avseth P., Mukerji T., and Mavko G., 2005 *Quantitative seismic interpretation.*Cambridge University Press.

[4] Backus G.E., 1962 *Long-wave elastic anisotropy produced by horizontal layering.* J Geophys Res 67:44274440.

[5] Carcione J. M., Santos J.E. y Picotti S., 2012 *Fracture-Induced Anisotropic Attenuation.* Rock Mech. Rock Eng., 45: 929-942.

[6] Carcione, J. M., 2015 *Wave fields in real media: Theory and numerical simulation of wave propagation in anisotropic, anelastic, porous and electromagnetic media.* 3rd ed.: Elsevier Science.

[7] Carcione, J. M., and P. Avseth, 2015 *Rock-physics templates for clay-rich source rocks.* Geophysics, 80, no. 5, D481–D500, doi: 10.1190/GEO2014-0510.1.

[8] Chopra, S. and Castagna, 2014 *AVO.*Society of Exploration Geophysicists, N° 16.

[9] Curcio A., Grosso A., Perez R., Barrios O., 2016 *Anisotropy study of deep unconventional reservoir inverting Walkaway VSP data, Argentina.*SEGAM2016-13577602.1.

[10] Curia D., Corti E., Pare A., Linares L., Paris M., 2016 *The Use of Walkaway and Walkaround VSP Surveys to Characterize HTI and VTI Anisotropy at the Vaca Muerta Formation.* SEGAM2016.

[11] Gauzellino P.M., Santos J.E. and Sheen D., 2001 *Frequency domain wave propagation modelling in exploration seismology.* Journal of Computational Acoustics, Vol 9 (3), 941–955.

[12] Gauzellino, P.M., Santos, J.E., Carcione J.M. and Picotti, S., 2014 *A rheological equation for anisotropic-anelastic media and simulation of field seismograms.* Wave Motion, Vol 51, 743–757.

[13] Grechka VA., Bakulin A., Tsvankin I., 2003 *Seismic characterization of vertical fractures described as general linear-slip interfaces.* Geophys Prospect 51:117130.

[14] Grechka VA.,Tsvankin I., 2003 *Feasibility of seismic characterization of multiple fracture sets.* Geophysics 68:13991407.

[15] Heidbach, O., Tingay, M., Barth, A., Reinecker, J., Kurfeb, D., Muller, B., 2008 *The World Stress Map database release 2008.* doi:10.1594/GFZ.WSM.Rel2008.

[16] Howell J.A., Schwarz E., Spalletti L.A., Veiga G.D. 2005 *The Neuqun Basin: an overview. In The Neuquén Basin, Argentina: A Case Study in Sequence Stratigraphy and Basin Dynamics.* Chap. 1, 1-14. Geological Society, London, Special Publications, 252.

[17] Li X., 1999 *Fracture detection using azimuthal variation of P-wave moveout from orthogonal seismic survey lines.* Geophysics, 64:11931201.

[18] Lindsay R., and Koughnet R.V., 2001 *Upscaling Well Logs to Seismic Wavelengths.* The Leading Edge, February 2001.

[19] Liu E., Martinez A., 2012 *Seismic Fracture Characterization: Concepts and Practical Applications.* EAGE Publications.

[20] Loucks, R. G., R. M. Reed, 2014 *Scanning-Electron-Microscope Petrographic Evidence for Distinguishing Organic-Matter Pores Associated with Depositacional Organic Matter versus Migrated Organic Matter in Mudrocks.* GCAGS Journal, v. 3, p. 5160.

[21] Nichols D., Muir F., Schoenberg M., 1989 *Elastic properties of rocks with multiple sets of fractures.* Geophysics, Extended Abstracts, pp 471474.

[22] Ostrander W.J., 1984 *Plane-wave reflection coefficients for gas sands at nonnormal angles of incidence.* Geophysics, 49, 1637-1648.

[23] Pinna, G., J. M. Carcione, and F. Poletto, 2011 *Kerogen to oil conversion in source rocks: Pore-pressure build-up and effects on seismic velocities.* Journal of Applied Geophysics, 74, 229–235, doi: 10.1016/j.jappgeo .2011.05.006.

[24] Pistre V.,Sinha B., 2008 *Applications of sonic waves in the estimation of petrophysical, geophysical and geomechanical properties of subsurface rocks.*IEEE International Ultrasonics Symposium Proceedings, doi: 10.1109/ULTSYM.2008.0020.

[25] Rasolofosaon P., Zinszner B., 2014 *Petroacoustics-Chapter 4: Elastic anisotropy.* IF-PEN, doi: 10.2516/ifpen/2014002.c004.

[26] Rezaee R., 2015 *Fundamentals of Shale Gas Reservoir.* Department of Petroleum Engineering Curtin University.

[27] Rodrigues N., Cobbold P. R., Loseth H., and Ruffet G., 2009 *Widespread bedding-parallel veins of fibrous calcite (beef) in a mature source rock (Vaca Muerta Fm, Neuquen Basin, Argentina): evidence for overpressure and horizontal compression.*Journal of the Geological Society, 166(4):695709.

[28] Rüger A., 2002 *Reflection coefficients and azimuthal AVO analysis in anisotropic media.* Society of Exploration Geophysicists.

[29] Russell B. H., 1988 *Introduction to seismic inversion methods.*Society of Exploration Geophysicists.

[30] Sánchez Camus A., Gauzellino P., Ramos R., 2016 *Modelado de medios anisótropos-Abaqus-CAE.* AAMCA- Mecánica Computacional Vol XXXIV, pgs. 1061-1077- Paper-4612.

[31] Sánchez Camus A., Gauzellino P., Ramos R., 2017 *Propagación de ondas elásticas en medios fracturados con anisotropía ortorrómbica.* AAGG 2017.

[32] Sayers, C. M., 2013 *The effect of anisotropy on the Young's moduli and Poisson's ratios of shales.* Geophysical Prospecting, 61, 416–426, doi: 10.1111/j.1365-2478.2012.01130.x.

[33] Sayers, C. M., 2013 *The effect of kerogen on the elastic anisotropy of organic-rich shales.* Geophysics, 78, D65–D74, doi:10.1190/GEO2012-0309.1.

[34] Schoenberg M., Muir F., 1989 *A calculus for finely layered anisotropic media.* Geophysics, 54:581589.

[35] Schoenberg M.,Muir F., Sayers C.M, 1996 *Introducing ANNIE: A simple three-parameter anisotropic velocity model for shales.*Journal of Seismic Exploration, 5, 3549.

[36] Schoenberg M., Helbig K., 1997 *Orthorhombic media: modeling elastic wave behavior in a vertically fractured earth.* Geophysics, 62:19541974.

[37] Sinha B.,Vissapragada B., Renlie L., Tysse S., 2006 *Radial profiling of the three formation shear moduli and its application to well completions.*Geophysics, 71, no. 6, P. E65E77, doi: 10.1190/1.2335879.

[38] Sone, H., and M. D. Zoback, 2013 *Mechanical properties of shale gas reservoir rocks-Part 1: Static and dynamic elastic properties and anisotropy.* Geophysics, 78,no. 5,D381D392 , doi: 10.1190/geo2013-0050.1.

[39] Swarbrick R.E., Osborne M.J., Yardley G.S., 2002 *Comparison of overpressure magnitude resulting from the main generating mechanisms. In: Pressure Regimes in Sedimentary Basins and Their Prediction.* AAPG Memoir, 76, 112.

[40] Thomsen, L., 1986 *Weak elastic anisotropy.* Geophysics, 51, 1954–1966, doi: 10.1190/1.1442051.

[41] Tsvankin I., 2005 *Seismic Signatures and Analysis of Reflection Data in Anisotropic Media.* Elsevier Science.

[42] Tsvankin I., Grechka V., 2011 *Seismology of Azimuthally Anisotropic Media and Seismic Fracture Characterization.* 17 Geophysical References Series, Society of Exploration Geophysicists.

[43] Vernik, L., and A. Nur, 1992 *Ultrasonic velocity and anisotropy of hydrocarbon source rocks.* Geophysics, 57, 727–735, doi: 10.1190/1.1443286.

[44] Vernik, L., 1994 *Hydrocarbon-generation-induced microcracking of source rocks.* Geophysics, 59, 555–563, doi: 10.1190/1.1443616.

[45] Vernik, L., and C. Landis, 1996 *Elastic anisotropy of source rocks: Implications for hydrocarbon generation and primary migration.* AAPG Bulletin, 80, 531–544.

[46] Vernik, L., and X. Liu, 1997 *Velocity anisotropy in shales: A petrophysical study.* Geophysics, 62, no. 2, 521–532, doi: 10.1190/1.1444162.

[47] Vernik, L., and J. Milovac, 2011 *Rock physics of organic shales.* The Leading Edge, 30, 318–323, doi: 10.1190/1.3567263.

[48] Walsh J., 2013 *The impact of the tool effect on polar anisotropy parameters derived from sonic waveform data.*SEG Technical Program Expanded Abstracts 2013: pp. 488-492.

[49] Willis M., Tutuncu A.N., 2014 *Geomechanical Integration of Core, Drilling, Microseismic and Well Log Data for Geomechanical Property Determination and Monitoring in the Argentinian Vaca Muerta Shale Formation.* URTeC: 1922481.

[50] Yenugu, M., and D.H. Han, 2013 *Seismic characterization of kerogen maturity: An example from Bakken shale.* 83rd Annual International Meeting, SEG, Expanded Abstracts, 2773–2777.

[51] Zoeppritz K., 1919 *On the reflection and propagation of seismic waves.*Erdbebenwellen VIIIB,Gttinger Nachrichten, I, 66-84.